Probing the electronic structure of tyrosine radial Y-D (center dot) in photosystem II by EPR spectroscopy using site specific isotope labelling in Spirodela oligorrhiza

Alia, A.; Hulsebosch, B.; Gorkom, H.J. van; Raap, J.; Lugtenburg, J.; Matysik, J.; ... ; Gast, P.

Available online at www.sciencedirect.com
SCIENCE DIRECT®
Chemical Physics 294 (2003) 459–469
Chemical Physics
www.elsevier.com/locate/chemphys

Probing the electronic structure of tyrosine radical $Y_D^{\bullet}$ in photosystem II by EPR spectroscopy using site specific isotope labelling in *Spirodela oligorrhiza* ☆

Alia [a,b,*], Bob Hulsebosch [a], Hans J. van Gorkom [a], Jan Raap [b], Johan Lugtenburg [b], Jörg Matysik [b], Huub J.M. de Groot [b], Peter Gast [a]

[a] *Department of Biophysics, Leiden Institute of Physics, Huygens Laboratory, Leiden University, P.O. Box 9504, 2300 RA Leiden, The Netherlands*
[b] *Leiden Institute of Chemistry, Gorlaeus Laboratoria, P.O. Box 9502, 2300 RA Leiden, The Netherlands*

Received 18 February 2003

Abstract

Tyrosine (Y_D) in the D2 reaction centre polypeptide of photosystem II (PSII) is redox-active and, under illumination, forms a dark-stable radical $Y_D^{\bullet}$. The origin of its stability and the functional role of $Y_D^{\bullet}$ are not well understood. For understanding the electronic structure and reactivity of $Y_D^{\bullet}$, it is crucial to unambiguously establish its hyperfine structure. There is considerable variation in the hyperfine data of $Y_D^{\bullet}$ and their interpretation in literature. In the present study, the hyperfine structure of tyrosine radical $Y_D^{\bullet}$ in PSII was probed by EPR in conjunction with carefully designed site specific isotope labelling. A comprehensive series of different selectively ^{2}H-, ^{13}C- or ^{17}O-labeled tyrosine were synthesized and incorporated in *Spirodela oligorrhiza* with more than 95% enrichment. The ^{13}C- and ^{17}O-hyperfine interactions were obtained from spectral simulations. From the anisotropy of the hyperfine interactions the spin densities at all phenoxyl ring positions were precisely obtained. Comparison of the absolute differences in individual spin densities between $Y_D^{\bullet}$ and neutral tyrosine radical in vitro with those of computationally calculated spin densities yield excellent agreement for a well ordered hydrogen bond between $Y_D^{\bullet}$ and the surrounding protein matrix with a bond length of 1.5 Å. Enantioselective labeling confirms that the β-methylene hydrogens of $Y_D^{\bullet}$ in *S. oligorrhiza* are oriented in a highly constrained specific position making $Y_D^{\bullet}$ strongly immobilized, thereby ensuring a firm hydrogen bond of the phenoxyl oxygen to the protein matrix.

Keywords: EPR; Tyrosine Y_D; Photosynthesis; Isotope labeling; Hyperfine interactions; Spin density; *Spirodela oligorrhiza*

Abbreviations: HFI, hyperfine interaction; P680, photooxidizable chlorophyll; PSII, photosystem II.

☆ Dedicated to the memory of Prof. Arnold J. Hoff. He was initiator of the work presented in this paper.

* Corresponding author. Tel.: +31-71-5274623; fax: +31-71-5274603.
E-mail address: alia@chem.leidenuniv.nl (Alia).

1. Introduction

The reaction centre of photosystem II (PSII) contains two redox-active tyrosine residues, designated Y_Z and Y_D, at positions 161 of the D1 and

0301-0104/$ - see front matter © 2003 Elsevier B.V. All rights reserved.
doi:10.1016/S0301-0104(03)00326-4

160 of the D2 polypeptide, respectively [1,2]. Their properties, reviewed in [3–5], are widely different. Y_Z is in the 'active branch' of the reaction centre, mediating electron transfer from the O_2 evolving Mn cluster to the oxidized reaction centre chlorophyll $P680^+$. Its midpoint potential must be near 1 V and even when the O_2 evolving complex is inactivated the oxidized form, the tyrosyl radical $Y_Z^{\cdot}$ lives at most a few seconds. Y_D is in the 'inactive branch' and normally remains in its oxidized state during photosynthesis as the stable neutral tyrosyl radical $Y_D^{\cdot}$. Like Y_Z, it can be oxidized by $P680^+$ in sub-μs times when its deprotonation is not rate-limiting [6], but its reduction in the dark can take hours [7] in spite of its high midpoint potential (titrated at 0.76 V [8]). Although Y_D does not participate in the steady-state electron transfer from water to $P680^+$, it is in slow equilibrium with the water-oxidizing complex: $Y_D^{\cdot}$ oxidizes the complex from its S_0 state to the S_1 state in tens of minutes [9], while Y_D will reduce the S_2 state to S_1 and the S_3 state to S_2 in a few seconds (see Ref. [10]). The functional role of $Y_D^{\cdot}$ might be in preventing disassembly of the Mn cluster by Mn^{2+} loss at night, and/or in preventing photo-oxidative damage during excess illumination by mediating an electron transfer cycle in PSII [11,12]. It has also been proposed that the redox potential of P680 is modulated by the redox state of Y_D [13], but in the case of $Y_Z^{\cdot}$, where a slightly decreased excitation trapping efficiency of the reaction centre by the oxidized tyrosine has in fact been reported, the rate of charge recombination was not increased [14].

The remarkable differences in potential and reactivity of $Y_Z^{\cdot}$ and $Y_D^{\cdot}$ are poorly understood. The stability of $Y_D^{\cdot}$ indicates that it resides in a highly isolated protein environment. ESEEM experiments showed that there is little variation in the orientation of the alkyl chain of $Y_D^{\cdot}$ with respect to its phenoxyl ring [15]. Moreover, enantioselective deuteration of the methylene group provided evidence that the $Y_D^{\cdot}$ phenoxyl ring is strongly immobilized in a constrained position [16] in *Synechocystis,* with a well-ordered hydrogen bond interaction between its phenol oxygen and a proton from D2 His-189 (in cyanobacteria; D2 His-190 in higher plants) [17]. Evidence for such a hydrogen bond comes from spectroscopic, molecular modeling, and mutagenesis studies [18,19] and seems more convincing than the assignment of D2 His-189 at a distance of 11.3 Å from Y_D in the recent X-ray structure [2] which would rule it out. At the current resolution of 3.7 Å, the assignment of individual amino acid residues in the X-ray structure is necessarily speculative.

For understanding the electronic structure and reactivity of $Y_D^{\cdot}$, it is crucial to establish the complete hyperfine structure and spin-density distribution of the unpaired π-electrons. The EPR spectrum of $Y_D^{\cdot}$ is largely characterized by its hyperfine interactions (HFI) as determined with EPR [20,21], ESEEM [15] and ENDOR [22] spectroscopy of the unpaired electron spin density with the nuclear magnetic moments of the 3′ and 5′ α-protons and one of the two so-called β-methylene protons (see Fig. 1A for the chemical structure and nomenclature). The isotropic β-methylene proton hyperfine interactions are via a hyperconjugative mechanism directly related to the orientation of the β-protons with respect to the plane of the tyrosine phenol ring and the spin-density at the nearest ring carbon C1′. Small alterations of this so-called dihedral angle θ of the β-protons, drastically influences the magnitude of the isotropic HFI and therefore basically determines the shape of the $Y_D^{\cdot}$ EPR spectrum. The lineshape is relatively insensitive to the smaller couplings of the system. Both the HFI and the spin-density distribution are suitable probes for protein-induced structural changes, providing for example information on the phenoxyl oxygen–carbon bond length, puckering of the phenoxyl ring [23–25], and the orientation of methylene β-protons [26,27]. There is considerable variation in the hyperfine data of $Y_D^{\cdot}$ and their interpretation in the literature [21]. Although the distribution of spin density over the tyrosine radical has been earlier obtained with the semi-empirical McConnell relations for isotropic proton HFI [28,29], accurate determination of the spin density at all positions could not be achieved. The density at the carbon C1′ is uncertain since it is related to the conformational angles of the β-methylene protons, which are difficult to obtain and may vary. There is uncertainty in the sign of the small densities at C2′ and C6′ positions of tyrosine. Proton ENDOR/EPR cannot distin-

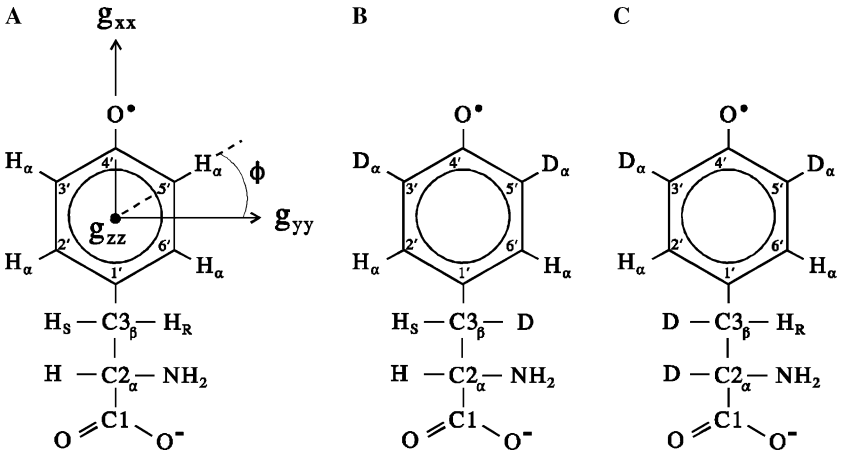

Fig. 1. Numbering scheme and directions of the principal axes of the *g*-tensor in the tyrosine radical. The Euler angle ϕ represents an in-plane rotation of the hyperfine components, defined in the molecular axes system, relative to the *g*-axes frame (A). Structure of (2*S*,3*R*)[3,3′,5′-$^2H_3$]-L-tyrosine (B) and (2*S*,3*S*)[2,3,3′,5′-$^2H_4$]-L-tyrosine (C).

guish between electron spin density at ring C4′ and the phenolic oxygen when the McConnell relations are employed, since neither atom has an attached proton. Earlier, isotopic enrichment of the tyrosine with ^{17}O combined with EPR spectral simulation has been used to determine the spin density at C4′, viz. 0.28 ± 0.01, in *Synechocystis* reaction centers [30]. In order to give a full unequivocal description of the spin-density distribution of $Y_D^{\bullet}$, we have applied incorporation of selectively ^2H-, ^{13}C-, and ^{17}O-enriched tyrosines in the higher plant *Spirodela* (*S.*) *oligorrhiza* (duckweed) in the present work. Most of the tyrosine phenol ring carbons, oxygen (C1′, C2′, C3′, C4′, C5′, C4′) and the β-methylene hydrogens were specifically labeled. Since ^{13}C-HFI are, with respect to proton HFI, more sensitive to changes of the spin density, ^{13}C-enrichment allows more accurate determination of the total spin-density distribution. Additional ^2H-labeling of the 3′ and 5′ positions was used to partially suppress the proton HFI, facilitating better observation of the other ^1H-, ^{13}C- and ^{17}O-HFI. Enantioselective deuteration of the β-methylene hydrogens (see Figs. 1B and C) yields the orientation of both hydrogens in *S. oligorrhiza*. The in vivo data of isotopically labelled $Y_D^{\bullet}$ in *S. oligorrhiza* are compared with data for isotopically labelled tyrosine radicals in alkaline frozen solution [31] and discussed in terms of differences in hydrogen bond interaction to the O_4' oxygen. Our results provide precise HFI and spin-density distribution on $Y_D^{\bullet}$ in PSII of *S. oligorrhiza* and clearly show that the conformation of the aromatic ring of $Y_D^{\bullet}$ is highly constrained and strongly immobilized, locking the phenoxyl ring in a fixed position, thereby ensuring a firm hydrogen bond of the phenoxyl oxygen to the protein matrix.

2. Materials and methods

2.1. Incorporation of ^2H-, ^{13}C- or ^{17}O-labeled tyrosine in S. oligorrhiza

Highly enriched selectively ^{13}C- (>98%) or ^{17}O-labeled (43%) tyrosine was synthesized as described [32]. Enantioselective deuteration of the β-methylene hydrogens was performed as described [33,34]. Additional deuteration of the tyrosine 3′ and 5′ α-hydrogens [35] was accomplished for a number of selected samples. As a result the following series of labeled tyrosine was used for bio-incorporation: [3′,5′-$^2H_2$]-L-tyrosine, [1′-$^{13}C_1$]-L-tyrosine, [1′-$^{13}C_1$; 3′,5′-$^2H_2$]-L-tyrosine, [2′-$^{13}C_1$]-L-tyrosine, [2′-$^{13}C_1$; 3′,5′-$^2H_2$]-L-tyrosine, [3′-$^{13}C_1$]-L-tyrosine, [3′,5′-$^{13}C_2$]-L-tyrosine, [4′-$^{13}C_1$]-L-tyrosine, [4′-$^{13}C_1$;

3′,5′-$^{2}H_2$]-L-tyrosine, [4′-$^{17}O_1$; 3′,5′-$^{2}H_2$]-L-tyrosine, (2*S*,3*R*) [3,3′,5′-$^{2}H_3$]-L-tyrosine and (2*S*,3*S*) [2,3,3′, 5′-$^{2}H_4$]-L-tyrosine (see Figs. 1B and C for the enantioselectively labeled tyrosines).

S. oligorrhiza was grown under aseptic conditions on half-strength Hutner's medium [36] under continuous light (20 μE m^{-2} s^{-1}) at 25 °C. The medium was continuously bubbled with sterile air containing 5% CO_2. A spontaneous tyrosine-tolerant plant of *S. oligorrhiza* was obtained by growing wild-type plants in half-strength Hutner's medium containing 40 mg/l tyrosine along with a mixture of other amino acids. This tyrosine-containing medium was found to be toxic for most wild-type *S. oligorrhiza*. A selected tyrosine-tolerant plant was subcultured on a medium containing increasing concentrations (up to 80 mg/l) of tyrosine. For labeling of *S. oligorrhiza*, a mixture of non-enriched amino acids [37] and the specific labeled tyrosine (75 mg/l) were added to the culture medium. 3–5 plants of tyrosine-tolerant *S. oligorrhiza* were inoculated in a culture flask containing 100 ml of culture medium. Plants were harvested when the surface of the medium was completely covered with plants (2–3 weeks later).

2.2. Sample preparation

Thylakoid membranes from *S. oligorrhiza* were isolated as described [38] using 25 mM Tricine buffer (pH 7.8) containing 15 mM NaCl, 5 mM $MgCl_2$ and 0.4 M sucrose. For the preparation of the EPR sample the membranes were resuspended in a 25 mM MES buffer (pH 7.8) containing 15 mM $CaCl_2$, 5 mM $MgCl_2$, 25% v/v glycerol and 3 mM Na-EDTA. For analysis of the extent of labeled tyrosine incorporation, the thylakoid membranes were hydrolyzed, [37] and the resulting amino acids were derivatized according to Husek [39] to increase the volatility of the amino acids. Gas-chromatography and electron impact mass spectrometry (GC-MS, GC Chrompack 25 m fused silica column, CP-sil-5CB 0.25 mm id.; MS ITD 700, Finnigan MAT) was used to determine the amount of incorporation. $Y_D^{\cdot}$ radicals were photoaccumulated by illuminating the EPR sample for a few seconds at room temperature. Prior to freezing in liquid nitrogen, the samples were kept in complete darkness for 3 min at room temperature to ensure disappearance of all radical species except for the long-lived $Y_D^{\cdot}$. In vitro tyrosine radicals were prepared in NaOD as described [31].

2.3. EPR measurements

X-band (9.2 GHz) EPR experiments were performed with a Varian E-9 spectrometer equipped with a 100 kHz field modulation unit. For all experiments a 0.25 mT field modulation was used. An Oxford Instruments flow cryostat provided cooling for experiments at low temperatures (95 K).

2.4. Simulations

All EPR spectra were simulated using a powder EPR simulation program based on that of Hoganson and Babcock [40], which takes into account the appropriate nuclear *g* values for ^{1}H, ^{2}H, ^{13}C, and ^{17}O, anisotropic HFIs and *g* values for upto eight nuclei, Euler angles, and spin packet line width parameters, as described in details earlier [31]. For the $Y_D^{\cdot}$ not deuterated at positions 3′ and 5′, best results were obtained with spin packet linewidth parameters of about 0.20 mT, while for the 3′ and 5′ deuterated $Y_D^{\cdot}$ a value of about 0.28 mT was used. The EPR spectrum of the [4′-$^{17}O_1$; 3′,5′-$^{2}H_2$]-labelled $Y_D^{\cdot}$ was simulated with spin packet linewidth of 0.52 mT. The variation in spin packet linewidth may be rationalized by a nuclear spin-dependent line broadening caused by different relaxation behaviour of the different nuclei [31]. The theory summarized in [31] was used to calculate the spin density from the anisotropy of the obtained ^{13}C- and ^{17}O-HFI tensors.

3. Results

Fig. 2 shows the gas chromatogram (A) and typical mass spectra of derivatized tyrosine obtained from *S. oligorrhiza* grown in the presence of [3′,5′-$^{13}C_2$]-L-tyrosine (B) and of unlabeled L-tyrosine (C). Two atomic mass unit difference

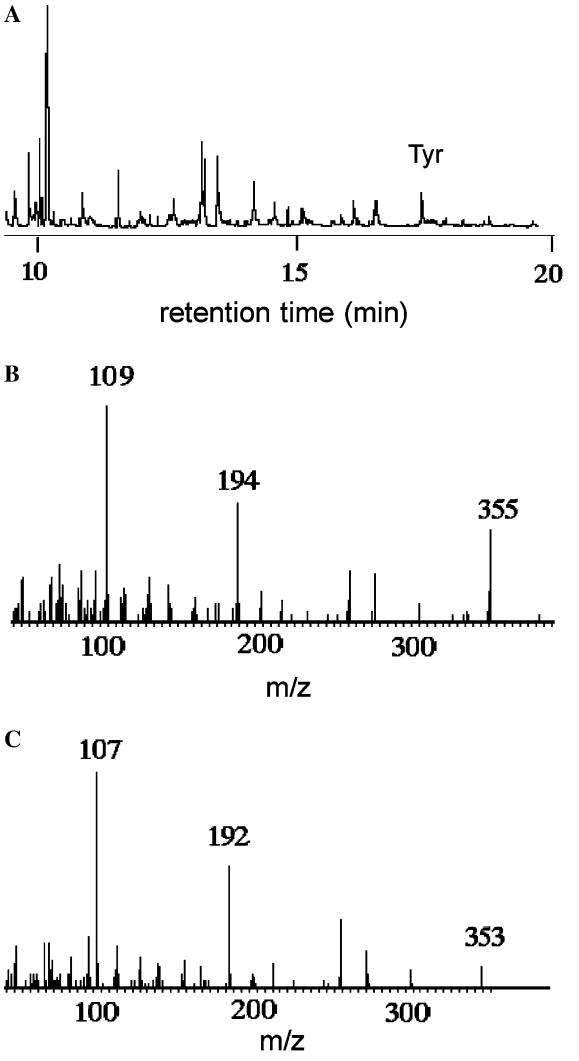

Fig. 2. Determination of the ^{13}C-isotope enrichment of tyrosine residues in *S. oligorrhiza* by GC-MS after hydrolysis of the protein and derivatization of tyrosine. (A) Gas chromatogram of a protein hydrolysate of [3′,5′-$^{13}C_2$]-L-tyrosine labeled *S. oligorrhiza* after derivatization. (B) Mass spectrum of derivatized [3′,5′-$^{13}C_2$]-L-tyrosine, (C) mass spectrum of derivatized unlabeled L-tyrosine.

between the labeled and unlabeled tyrosine residue is clearly visible. For this specific sample as well as for the other samples an average of $95 \pm 5\%$ uptake of the labeled tyrosine was accomplished.

Figs. 3 and 4 show the collected experimental (solid line) and simulated (dashed line) X-band (9.2 GHz) EPR spectra of isotope-labeled $Y_D^{\cdot}$ radicals

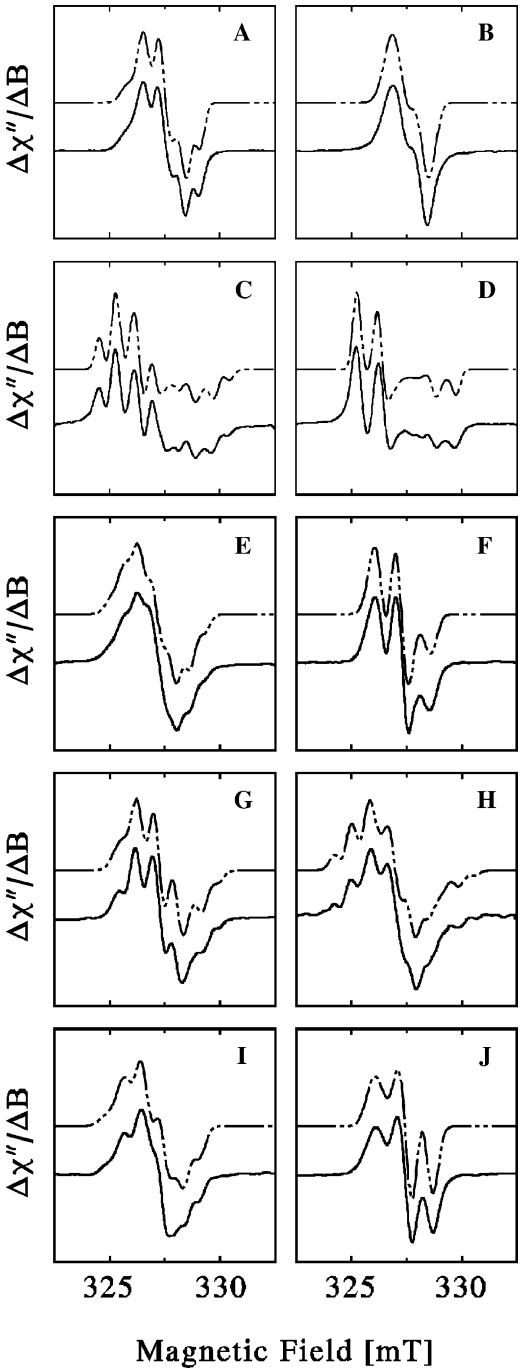

Fig. 3. Experimental (solid line) and simulated (dashed line) X-band (9.2 GHz) spectra of labeled $Y_D^{\cdot}$ in *S. oligorrhiza*. Unlabeled, (A); [3′,5′-$^2H_2$]-, (B); [1′-$^{13}C_1$]-, (C); [1′-$^{13}C_1$, 3′,5′-$^2H_2$]-, (D); [2′-$^{13}C_1$]-, (E); [2′-$^{13}C_1$, 3′,5′-$^2H_2$]-, (F); [3′-$^{13}C_1$]-, (G); [3′,5′-$^{13}C_2$]-, (H); [4′-$^{13}C_1$]-, (I); [4′-$^{13}C_1$, 3′,5′-$^2H_2$]-, (J).

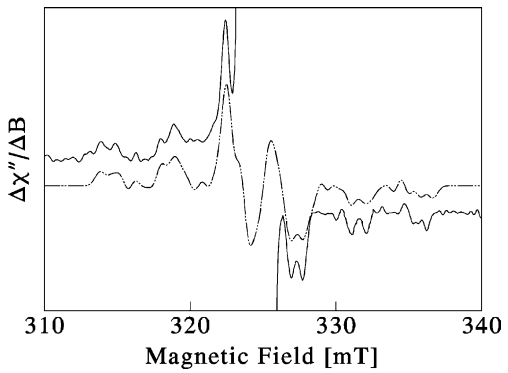

Fig. 4. Experimental (solid line) and simulated (dashed line) X-band (9.2 GHz) spectra of [4′-$^{17}O_1$, 3′,5′-$^2H_2$]-labeled $Y_D^{\cdot}$ in *S. oligorrhiza*.

in PSII of *S. oligorrhiza*. As expected from the GC-MS experiments, no trace of unlabeled tyrosine radicals is visible in the EPR spectra. The $Y_D^{\cdot}$ ^{1}H-, ^{13}C-, ^{17}O-HFI tensor components, A_{xx}, A_{yy} and A_{zz}, obtained from the simulations, together with the calculated isotropic hyperfine value (A_{iso}) and the dipolar couplings (D_{xx}, D_{yy}, D_{zz}) are given in Table 1. Best simulations of the spectra were obtained using an angle ϕ of $25° \pm 2$ °C for positions 2, 3, 5, and 6, where ϕ is the Euler angle transforming the hyperfine components, defined in the molecular system, to the *g*-axes system (Fig. 1). Normally, assuming a regular hexagonal aromatic ring structure, one would expect an angle ϕ of 30° instead of $25° \pm 2$ °C. This relatively large deflection in the Euler angle of $Y_D^{\cdot}$ in duckweed compared to theoretical value may result from a change in bond angle of C–H proton, due to steric hindrance from the protein environment, or from a ring structure distortion. The *g*-tensor was: $g_{xx} = 2.0076 \pm 0.0002$, $g_{yy} = 2.0045 \pm 0.0002$, $g_{zz} = 2.0023 \pm 0.0002$, slightly different from the in vitro tyrosine radical [31]. For the simulations a spin packet linewidth parameter of 0.20 mT or 0.28 mT was used for the protonated or deuterated samples, respectively. Note that for almost each set of simulation parameters two spectra ($Y_D^{\cdot}$ with and without 3′,5′-$^2H_2$ labeling) had to be simulated. In the following paragraphs we shall briefly discuss the characteristics of each selectively labeled $Y_D^{\cdot}$ in *S. oligorrhiza*.

3.1. [1′-$^{13}C_1$]-Tyrosine $Y_D^{\cdot}$

For accurate determination of the spin density at C1′, without being dependent on the conformational variability of the methylene protons, [1′-$^{13}C_1$]-labeled tyrosine was incorporated into PSII. As shown in Fig. 3C, large ^{13}C-HFI are observed from [1′-$^{13}C_1$] labelled $Y_D^{\cdot}$ radicals in *S. oligorrhiza* suggesting that the spin density at C1′ is relatively high. From the dipolar interactions a spin density of 0.32 ± 0.01 was calculated. From the calculated spin density at C1′, the dihedral angles of the methylene protons were determined using the McConnell relation and were found to be 47° and 73°. Following [15], an angular distribution of ±2° around these central angles was used in the simulations. The dihedral angles thus obtained were kept fixed for the simulation of the spectra from other labelled $Y_D^{\cdot}$ samples. This procedure allowed the accurate determination of all HFI (Table 1).

3.2. [2′-$^{13}C_1$]-Tyrosine $Y_D^{\cdot}$

Determination of the low spin density at C2′ is hampered by interference from the high densities at C1′ and C3′. Therefore, first the spin density at C3′ was determined (see below). Including the interactions with the spin density at C1′ and C3′, a spin density of -0.05 ± 0.01 at C2′ was calculated.

3.3. [3′-$^{13}C_1$]-Tyrosine $Y_D^{\cdot}$

From the anisotropy of the obtained HFI a spin density of 0.21 ± 0.01 was found at C3′. The interactions with the neighbouring spin densities are small and were neglected.

3.4. [4′-$^{13}C_1$]-Tyrosine $Y_D^{\cdot}$

C4′ is one of the blind spots in the determination of the total $Y_D^{\cdot}$ spin-density distribution. The observed ^{13}C-HFI is nearly isotropic, indicating a low density at C4′. Again, the influence of the high spin densities at C3′, C5′ *and* O4′ had to be taken into account for the calculation of the spin density at C4′ from the dipolar interactions. This resulted in a spin density of 0.03 ± 0.01 for this position.

Table 1
^{1}H-, ^{13}C-, and ^{17}O-HFI (in mT) for $Y_D^{\bullet}$ in *S. oligorrhiza* and tyrosine radicals in vitro

Atom	$Y_D^{\bullet}$ in *S. oligorrhiza*				In vitro [31]			
	ϕ	A_{xx} A_{yy} A_{zz}	D_{xx} D_{yy} D_{zz}	A_{iso}	ϕ	A_{xx} A_{yy} A_{zz}	D_{xx} D_{yy} D_{zz}	A_{iso}
C1′	0	−0.20 −0.20 3.45	−1.22 −1.22 2.43	1.02	0	−0.30 −0.30 3.40	−1.23 −1.23 2.47	0.93
C2′	25	−0.50 −0.75 −1.25	0.33 0.08 −0.42	−0.83	30	−0.65 −0.80 −1.20	0.23 0.08 −0.32	−0.88
C3′	−25	−0.50 −0.50 1.90	−0.80 −0.80 1.60	0.30	−23	−0.60 −0.60 2.00	−0.87 −0.87 1.73	0.27
C4′	0	−1.00 −1.10 −0.80	−0.03 −0.13 0.17	−0.97	0	−1.10 −1.20 −0.65	−0.12 −0.22 0.33	−0.98
C5′	25	−0.40 −0.40 2.10	−0.83 −0.83 1.67	0.43	23	−0.60 −0.60 2.00	−0.87 −0.87 1.73	0.27
O4′	0	0.60 0.60 −4.35	1.65 1.65 −3.30	−1.05	0	0.50 0.70 −4.07	+1.46 +1.66 −3.11	−0.96
H2′	25	0.17 0.27 0.04	0.01 0.11 −0.12	0.16	30	0.17 0.27 0.04	0.01 0.11 −0.12	0.16
H3′	−25	−1.04 −0.33 −0.68	−0.36 0.35 0.00	−0.68	−23	−0.96 −0.28 −0.70	−0.32 0.36 −0.06	−0.64
H5′	25	−0.98 −0.33 −0.68	−0.30 0.35 0.00	−0.68	23	−0.96 −0.28 −0.70	−0.32 0.36 −0.06	−0.64
H6′	−25	0.17 0.27 0.04	0.01 0.11 −0.12	0.16	−30	0.17 0.27 0.04	0.01 0.11 −0.12	0.16
H_R	0		0.80–0.93		0		0.00–0.46	
H_S	0		0.12–0.20		0		0.46–0.39	

Estimated errors vary between 0.02 and 0.07 mT for all HFI. The error in the Euler angles is estimated to be ±2°.

3.5. *[4′-$^{17}O_1$]-Tyrosine $Y_D^{\bullet}$*

The isotope ^{17}O has spin 5/2, resulting in a sixfold splitting of the EPR lines (Fig. 4). The combined ^{17}O- and [3′,5′-$^{2}H_2$]-labeling allowed us to resolve the structure of the central lines, and resulted in the accurate simulation of the respective spectra. Fig. 4 shows the experimental (solid line) and simulated (dashed line) X-band EPR spectrum of [4′-$^{17}O_1$; 3′,5′-$^{2}H_2$]-Tyrosine $Y_D^{\bullet}$. The central part of the experimental spectrum, corresponding to non-^{17}O-labeled $Y_D^{\bullet}$, was left out. The

^{17}O-HFI tensor components obtained are 0.6 ± 0.1 mT, 0.6 ± 0.1 mT and -4.35 ± 0.05 mT for A_{xx}, A_{yy} and A_{zz}, respectively, resulting in a spin density at O4′ of 0.28 ± 0.01. Similar values have been reported for $Y_D^{\cdot}$ in *Synechocystis* sp. ($A_{xx} = 0.5 \pm 0.2$ mT, $A_{yy} = 0.5 \pm 0.2$ mT, $A_{zz} = \sim 4.32 \pm 0.05$ mT) [30].

3.6. [5′-$^{13}C_1$]-Tyrosine $Y_D^{\cdot}$

Despite the high symmetry of $Y_D^{\cdot}$, the spin density at C5′ is found to be slightly larger than that of C3′. Spin density at C5′ was calculated to be 0.22 ± 0.01.

3.7. [6′-$^{13}C_1$]-Tyrosine $Y_D^{\cdot}$

A selectively labeled [6′-^{13}C$_1$]-tyrosine was not available. From the simulations of spectra for $Y_D^{\cdot}$ labeled at other positions, we find that the spin density at C6′ is -0.05 ± 0.01.

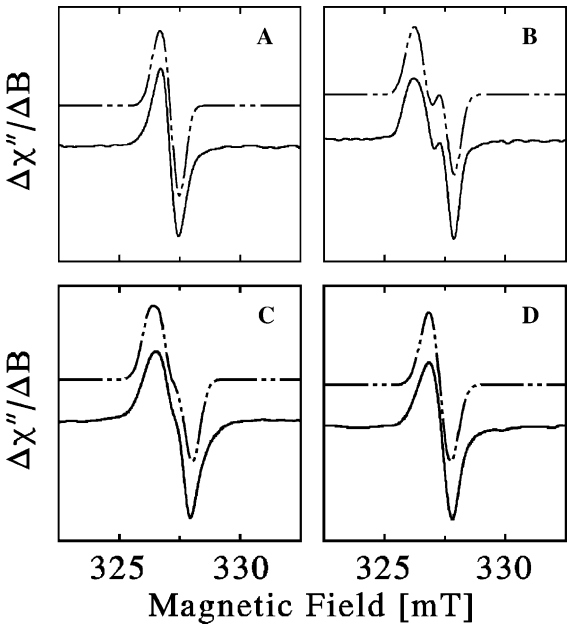

Fig. 5. Experimental (solid line) and simulated (dashed line) X-band (9.2 GHz) spectra of (2*S*,3*R*)[3,3′,5′-^{2}H$_3$]-, (A) and (2*S*,3*S*)[2,3,3′,5′-^{2}H$_4$]-, (B) labeled $Y_D^{\cdot}$ in *S. oligorrhiza*, or in vitro (C) and (D).

The sum of the spin densities at all positions is 0.96 ± 0.03, slightly lower than unity. Residual spin density is expected at the protons (small) and the C_α and C_β carbons of the alanine residue of tyrosine.

EPR spectra of $Y_D^{\cdot}$ with an enantioselective deuterated methylene group are shown in Fig. 5. The use of enantioselective deuteration of the β-hydrogens allows unequivocal assignment of the dihedral angle for each of the hydrogens, H_R and H_S. Simulation of the spectra indicates that H_R is related to the 47° dihedral angle, whereas the dihedral angle for H_S is 73°. Similar to $Y_D^{\cdot}$ in *Synechocystis* sp. PCC 6803 cells, the dihedral angles of the methylene group hydrogens are shifted by about 30° with respect to those of tyrosine radicals in vitro [16].

4. Discussion

In this work, a comprehensive series of site specific isotope labelled (^{2}H-, ^{13}C- and ^{17}O-enriched) tyrosines were successfully incorporated in PSII of *S. oligorrhiza* with >95% enrichment (Fig. 2). The complete description of the spin density distribution, the principle elements and approximate orientation of the hyperfine tensors of a number of carbon and proton positions of $Y_D^{\cdot}$ in PSII of *S. oligorrhiza* could be derived from simulation of the EPR spectra (Figs. 3 and 4; Tables 1 and 2). A comparison of $Y_D^{\cdot}$ in PSII (present work) with those of the neutral tyrosyl radical in vitro [31] shows small differences in hyperfine structure that can be related to hydrogen bond interaction of $Y_D^{\cdot}$ with the protein matrix. Previous studies have shown a moderate,

Table 2
Spin-density distributions of tyrosine radicals ($\rho = \pm 0.01$)

Atom	$Y_D^{\cdot}$	In vitro [31]	Theoretical [41]
C1′	0.32	0.32	0.31
C2′	−0.05	−0.04	−0.05
C3′	0.21	0.23	0.21
C4′	0.03	0.05	0.03
C5′	0.22	0.23	0.22
C6′	−0.05	−0.04	−0.05
O4′	0.28	0.26	0.29

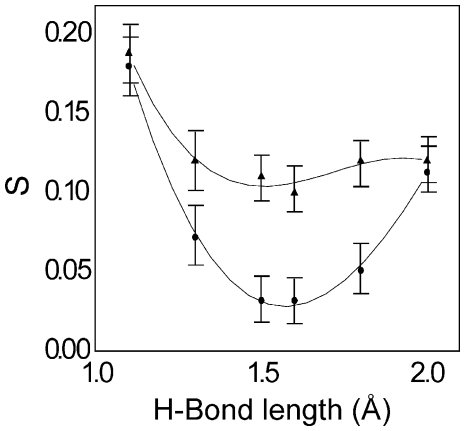

Fig. 6. $\sum S$ of the absolute differences in individual spin densities of $Y_D^{\cdot}$ in *S. oligorrhiza*, and in vitro tyr$^{\cdot}$ as a function of hydrogen bond length.

well-ordered hydrogen bond interaction of $Y_D^{\cdot}$ with D2 His 189 in *Synechocystis* 6803 [17], whereas the, distance of ~11.3 Å between $Y_D^{\cdot}$ and D2-His 189 in the recent X-ray structure of PSII, would not support D2-His189 as H-bonding partner of $Y_D^{\cdot}$ [2]. One of the aims of the present investigation was to assess the hydrogen bond of the phenoxyl oxygen of $Y_D^{\cdot}$ in PSII. In [41], a density functional theoretical study of the electronic structure of *p*-methylphenoxyl radical as a function of its hydrogen bond distance was presented. We examined the $\sum S$ of the absolute differences in individual spin densities between $Y_D^{\cdot}$ and those calculated for the *p*-methylphenoxyl radical in vacuo [41] for different strengths of hydrogen bond by using the following eq: $\sum |\rho_i(Y_D^{\cdot}) - \rho_i(\text{calculated})|$, $i = C_1 \ldots C_6, O_4$. Calculated values were obtained from [41]. This procedure provides a statistical average of the individual errors (similar to least square analysis). The value of S of $Y_D^{\cdot}$ and in vitro Tyr$^{\cdot}$ is plotted as a function of hydrogen bond length in Fig. 6. As can be seen from this figure, the minimum of S for Tyr$^{\cdot}$ in vitro, is less pronounced compared to $Y_D^{\cdot}$. This suggest that in $Y_D^{\cdot}$ of PSII, the hydrogen bond is well defined, with a bond length r_H close to 1.50 ± 0.3 Å, whereas in Tyr$^{\cdot}$ in vitro, the hydrogen bond is not well defined and distributed with r_H in the range of 1.3–2.0 Å. Thus our data support a well-ordered hydrogen bond between $Y_D^{\cdot}$ and the protein matrix. The value of hydrogen bond length for $Y_D^{\cdot}$ (1.5 Å) is close to the bond length calculated earlier from the g_{xx}-value as determined with high-field EPR experiments on spinach $Y_D^{\cdot}$ (~1.7 Å) [42]. The different hydrogen bond interactions of $Y_D^{\cdot}$ and of Tyr$^{\cdot}$ in vitro is also reflected in

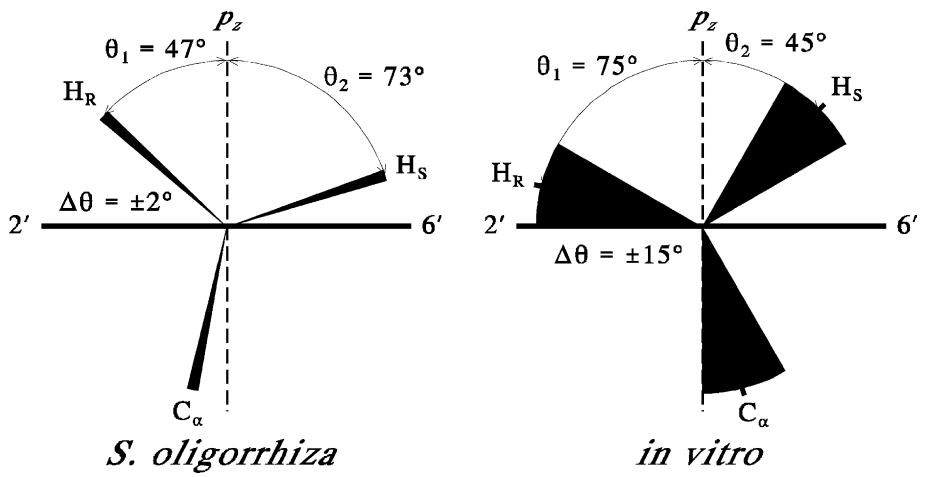

Fig. 7. Orientations of the phenoxyl ring relative to the methylene group for *S. oligorrhiza* and in vitro. The prochiral β-methylene hydrogens are indicated as H_R and H_S. The plane of the aromatic ring (horizontal line between 2′ and 6′ positions) is perpendicular to the plane of the paper; the view is down the $C3_\beta$–C1′ bond. θ_1 and θ_2 represent the dihedral angles between the $2p_z$ orbital at C1′ and the planes containing the C1′–$C3_\beta$–H_R bonds and the C1′–$C3_\beta$–H_S bonds, respectively. The conformational distributions of θ_1 and θ_2 for both systems are indicated.

especially the D_{zz} components of ^{13}C- and ^{17}O-hyperfine tensor (Table 1). Our experimental data are also in good agreement with the calculated ^{13}C-, and ^{17}O-hyperfine tensor components [43].

The orientation of the methylene hydrogens H_R and H_S for $Y_D^{\cdot}$ in *S. oligorrhiza* and for tyrosine radicals in vitro is compared in Fig. 7. Clearly visible are the different conformational distributions and orientations of H_R with respect to H_S in the two systems. In *S. oligorrhiza* the H_R-hydrogen is responsible for the largest of the two β-hydrogen HFI, whereas for the in vitro system the main interaction is due to H_S. Similar to $Y_D^{\cdot}$ in *Synechocystis,* the orientation with respect to the peptide moiety of the phenoxyl ring in *S. oligorrhiza* is locked in one particular position. There is, however, a small difference in the dihedral angles of the β-methylene hydrogens in both systems. For *S. oligorrhiza*, $\theta_1 = 47 \pm 2°$ and $\theta_2 = 73 \pm 2°$, whereas for *Synechocystis sp.* PCC 6803 $\theta_1 = 52 \pm 2$ and $\theta_2 = 68 \pm 2°$ [14]. The constrained orientation of $Y_D^{\cdot}$ found in cyanobacteria earlier and in higher plants in the present work may be important for its functioning in RCs of PSII; it may also be related to the unusual stability of the $Y_D^{\cdot}$ radical.

5. Conclusions

We have succeeded in incorporating highly enriched isotope-labeled tyrosine in a tyrosine-tolerant strain of the higher plant *S. oligorrhiza*. Numerous differently ^{13}C- and ^{17}O-labeled tyrosine $Y_D^{\cdot}$ radicals have been studied with X-band EPR to probe its precise electronic structure. Spectral simulations have yielded the ^{13}C- and ^{17}O-HFI tensors and allowed us to obtain the complete free electron spin-density distribution of $Y_D^{\cdot}$ in *S. oligorrhiza*. In comparison with tyrosine radicals in vitro, a small but significant redistribution of spin density has taken place. Comparison of sum of the absolute differences in individual spin densities between $Y_D^{\cdot}$ with those of computationally calculated spin densities yield excellent agreement for a well ordered hydrogen bond between $Y_D^{\cdot}$ and the protein matrix with a bond length of ~1.5 Å. Enantioselective deuteration of each of the two β-hydrogen show that the methylene group of the tyrosine radical in *S. oligorrhiza* is oriented in a specific constrained position. The precise information about the electronic structure of $Y_D^{\cdot}$ in PSII using comprehensive series of site directed isotope labelling presented in this work opens up the possibility to approach the electronic structure of $Y_Z^{\cdot}$ in PSII by the same strategy in future.

Acknowledgements

We thank Ineke de Boer for technical assistance. This research was supported by Netherlands Organization for Scientific Research (NWO) via the section Earth and Life Science (ALW). Alia acknowledges financial support by NWO via the CW PIONIER programme to HJMdG and via a Jonge Chemici grant to JM.

References

[1] A. Zouni, H.-T. Witt, J. Kern, P. Fromme, N. Krauß, W. Saenger, P. Orth, Nature 409 (2001) 739.
[2] N. Kamiya, J.-R. Shen, Proc. Natl. Acad. Sci. USA 100 (2003) 98.
[3] B.A. Diner, G.T. Babcock, in: D.R. Ort, C.F. Yocum (Eds.), Oxygenic Photosynthesis: The Light Reaction, Kluwer Academic Publishers, Dordrecht, 1996, p. 213.
[4] B.A. Diner, Biochim. Biophys. Acta 1503 (2001) 147.
[5] R.J. Debus, Biochim. Biophys. Acta 1503 (2001) 164.
[6] P. Faller, R.J. Debus, K. Brettel, M. Sugiura, A.W. Rutherford, A. Boussac, Proc. Natl. Acad. Sci. USA 98 (2001) 14368.
[7] G.T. Babcock, K. Sauer, Biochim. Biophys. Acta 376 (1975) 315.
[8] A. Boussac, A.L. Etienne, Biochim. Biophys. Acta 776 (1984) 576.
[9] I. Vass, S. Styring, Biochemistry 30 (1991) 830.
[10] Z. Deák, I. Vass, S. Styring, Biochim. Biophys. Acta 1185 (1994) 65.
[11] M. Rova, F. Mamedov, A. Magnuson, P.O. Frederiksson, S. Styring, Biochemistry 37 (1998) 11039.
[12] J. Lavaud, H.J. van Gorkom, A.L. Etienne, Photosynth. Res. 74 (2002) 51.
[13] B.A. Diner, F. Rappaport, Annu. Rev. Plant Biol. 53 (2002) 551.
[14] R. de Wijn, H.J. van Gorkom, Biochim. Biophys. Acta 1553 (2002) 302.
[15] K. Warncke, J. McCracken, G.T. Babcock, J. Am. Chem. Soc. 116 (1994) 7332.

[16] S.A.M. Nieuwenhuis, R.J. Hulsebosch, J. Raap, P. Gast, J. Lugtenburg, A.J. Hoff, J. Am. Chem. Soc. 120 (1998) 829.
[17] K.A. Campbell, J.M. Peloquin, B.A. Diner, X.-S. Tang, D.A. Chisholm, R.D. Britt, J. Am. Chem. Soc. 119 (1997) 4787.
[18] R.J. Debus, B.A. Barry, J.T. Babcock, L. McIntosh, Proc. Natl. Acad. Sci. USA 85 (1988) 427.
[19] X.-S. Tang, D.A. Chisholm, G.C. Dismukes, G.W. Brudvig, B.A. Diner, Biochemistry 32 (1993) 13742.
[20] B.A. Barry, M.K. El-Deeb, P.O. Sandusky, G.T. Babcock, J. Biol. Chem. 265 (1990) 20139.
[21] W. Hofbauer, A. Zouni, R. Bittl, J. Kern, P. Orth, F. Lendzian, P. Fromme, H.T. Witt, W. Lubitz, Proc. Natl. Acad. Sci. USA 98 (2001) 6623.
[22] S.E.J. Rigby, J.H.A. Nugent, P.J. O'Malley, Biochemistry 33 (1994) 1734.
[23] D.M. Chipman, R. Liu, X. Zhou, P. Pulay, J. Chem. Phys. 100 (1994) 5023.
[24] D.R. Armstrong, C. Cameron, D.C. Nonhebel, P.G. Perkins, J. Chem. Soc. Perkin Trans. II (1983) 569.
[25] Y. Shinagawa, J. Am. Chem. Soc. 100 (1978) 67.
[26] C. Tommos, X.-S. Tang, K. Warncke, C.W. Hoganson, S. Styring, J. McCracken, B.A. Diner, G.T. Babcock, J. Am. Chem. Soc. 117 (1995) 10325.
[27] K. Warncke, G.T. Babcock, J. McCracken, J. Chem. Phys. 100 (1994) 4654.
[28] H.M. McConnell, J. Chem. Phys. 24 (1956) 764.
[29] H.M. McConnell, D.B. Cheshunt, J. Chem. Phys. 28 (1958) 107.
[30] F. Dole, B.A. Diner, C.W. Hoganson, G.T. Babcock, R.D. Britt, J. Am. Chem. Soc. 119 (1997) 11540.
[31] R.J. Hulsebosch, J.S. van den Brink, S.A.M. Nieuwenhuis, P. Gast, J. Raap, J. Lugtenburg, A.J. Hoff, J. Am. Chem. Soc. 119 (1997) 8685.
[32] C. Winkel, M.W.M.M. Aarts, F.R. Van der Heide, E.G. Buitenhuis, J. Lugtenburg, Recl. Trav. Chim. Pays-Bas 108 (1989) 139.
[33] S.A.M. Nieuwenhuis, C. Mul, N.J. Van Belle, J. Lugtenburg, J. Raap, in: P. Mathis (Ed.), Photosynthesis, From Light to Biosphere, vol. II, Kluwer Academic Publishers, Dordrecht, 1995, p. 313.
[34] S.A.M. Nieuwenhuis, Doctoral Thesis, Leiden University, 1998.
[35] B. Lindström, B. Sjöquist, E. Anggard, J. Labelled Compd. 10 (1974) 187.
[36] H.B. Posner, in: F.A. Witt, S.N.K. Wessels (Eds.), Methods in Developmental Biology, Crowell, New York, 1967, p. 301.
[37] J. Raap, C. Winkel, A.H.M. De Wit, A.H.H. Van Houten, A.J. Hoff, J. Lugtenburg, Anal. Biochem. 191 (1990) 9.
[38] Alia, P.P. Saradhi, P.P. Mohanty, Biochem. Biophys. Res. Commun. 181 (1991) 1238.
[39] P.J. Husek, Chromatography 552 (1991) 289.
[40] C.W. Hoganson, G.T. Babcock, Biochemistry 31 (1992) 11874.
[41] C.T. Farrar, G.J. Gerfen, R.G. Griffin, D.A. Force, R.D. Britt, J. Phys. Chem. B 101 (1997) 6634.
[42] S. Un, M. Atta, M. Fontecave, A.W. Rutherford, J. Am. Chem. Soc. 117 (1995) 10713.
[43] P.J. O'Malley, D. Ellson, Biochim. Biophys. Acta 1320 (1997) 65.